Origin of broad NIR photoluminescence in bismuthate glass and Bi-doped glasses at room temperature

2009 J. Phys.: Condens. Matter 21 285106

(http://iopscience.iop.org/0953-8984/21/28/285106)

J. Phys.: Condens. Matter **21** (2009) 285106 (6pp) doi:10.1088/0953-8984/21/28/285106

Origin of broad NIR photoluminescence in bismuthate glass and Bi-doped glasses at room temperature

Mingying Peng, Cordt Zollfrank and Lothar Wondraczek

Lehrstuhl für Glas und Keramik, WW3, Friedrich Alexander Universität Erlangen-Nürnberg, Martensstrasse 5, D-91058 Erlangen, Germany

E-mail: mingying.peng@ww.uni-erlangen.de and lothar.wondraczek@ww.uni-erlangen.de

Received 8 December 2008, in final form 8 June 2009
Published 19 June 2009
Online at stacks.iop.org/JPhysCM/21/285106

Abstract

Bi-doped glasses with broadband photoluminescence in the near-infrared (NIR) spectral range are presently receiving significant consideration for potential applications in telecommunications, widely tunable fiber lasers and spectral converters. However, the origin of NIR emission remains disputed. Here, we report on NIR absorption and emission properties of bismuthate glass and their dependence on the melting temperature. Results clarify that NIR emission occurs from the same centers as it does in Bi-doped glasses. The dependence of absorption and NIR emission of bismuthate glasses on the melting temperature is interpreted as thermal dissociation of Bi_2O_3 into elementary Bi. Darkening of bismuthate glass melted at 1300 °C is due to the agglomeration of Bi atoms. The presence of Bi nanoparticles is confirmed by transmission electron microscopy, high-resolution energy dispersive x-ray spectroscopy and element distribution mapping. By adding antimony oxide as an oxidation agent to the glass, NIR emission centers can be eliminated and Bi^{3+} is formed. By comparing with atomic spectral data, absorption bands at ∼320 , ∼500 , 700 , 800 and 1000 nm observed in Bi-doped glasses are assigned to Bi^0 transitions $^4S_{3/2} \rightarrow {}^2P_{3/2}$, $^4S_{3/2} \rightarrow {}^2P_{1/2}$, $^4S_{3/2} \rightarrow {}^2D_{5/2}$, $^4S_{3/2} \rightarrow {}^2D_{3/2}(2)$ and $^4S_{3/2} \rightarrow {}^2D_{3/2}(1)$, respectively, and broadband NIR emission is assigned to the transition $^2D_{3/2}(1) \rightarrow {}^4S_{3/2}$.

(Some figures in this article are in colour only in the electronic version)

1. Introduction

Spectroscopic properties of Bi^{3+} and Bi^{2+} ions as activators or sensitizers in inorganic oxide host materials have been investigated extensively over the last four decades [1–7]. While excitation and emission properties of these ions strongly depend on the host lattice, they are usually found in the ultraviolet (UV) to visible (VIS) spectral range, and their fluorescence lifetime is hardly larger than 20 μs. It is only recently, however, that Murata *et al* [8] discovered a novel type of Bi-doped silicate glass that exhibits NIR emission at ∼1132 nm with a bandwidth (FWHM) of ∼150 nm and a lifetime of ∼650 μs. In the following and until today, for its significance to applications related to telecommunications and optical amplification in a broader sense, this class of Bi-doped materials has become the subject of extensive research. Broadband NIR emission has now been shown in Bi-doped silicate [8–11], germanate [12–16], borate [17], phosphate [18] and chalcogenide [19] glasses. Contrary to conventional Bi^{3+}- or Bi^{2+}-doped optical materials [1–7], up to five absorption bands (∼320, 500, 700, 800 and 1000 nm) can be present in these glasses and emission usually occurs in the spectral range of ∼1.0–1.6 μm. While the typical FWHM of emission is in the range of 150–300 nm, even higher bandwidths up to 500 nm have been reported (e.g. [11]). The observed fluorescence lifetime is typically longer than 200 μs [8–19].

Good overlap between the emission properties of these glasses and the optical loss spectrum of silica fibers implies application in ultrabroadband fiber amplifiers for telecommunication purposes. Furthermore, its use as a material for widely tunable lasers is presently being evaluated (e.g. [20]).

On the other hand, the fundamental origin of NIR emission is still subject to intensive debate [8–20]. This lack of understanding is more and more impeding further development and optimization of Bi-doped optical materials. That is, the valence in which the bismuth ion is optically active in the NIR remains disputed. Recent proposals include Bi^{5+}, Bi^{+} and Bi-based clusters [8–20]. Fujimoto *et al* originally assigned Bi^{5+} ions as NIR emission centers [10] and recently confirmed the presence of Bi^{5+} species in NIR-luminescent Bi-doped aluminosilicate glasses by x-ray absorption fine structure analysis (XAFS) [21]. But, at the same time, experimental results reported by other researchers showed a rather disparate trend towards Bi ions in low valence states [9, 11–20] According to Duffy's [22] theory of optical basicity, the increasing basicity of the host glass will facilitate formation of higher valence states of Bi. However, doing so experimentally by changing the composition of the base glass led to the weakening or even total disappearance of NIR photoluminescence [16, 17, 23]. In contrast, the introduction of reducing agents such as carbon into the batch (e.g. Ohishi *et al* [24]) clearly improved NIR emission intensity from Bi-doped soda lime silicate glass. Truong *et al* [25] found similar results when heat-treating Bi-doped silicate glass in a H_2 atmosphere.

Based on the assumption that, at high temperatures, Bi_2O_3 can dissociate into elementary Bi, Bi-based clusters have been discussed as potential NIR emission centers [14, 24–26]. On the other hand, recent experiments on NIR photoluminescence in bismuthate glasses, induced by femtosecond (fs) laser irradiation, suggested that the interaction time between the femtosecond laser and the glass was too short for clusters to form [27].

In the present study, bismuthate (Bi-rich) glasses were considered, and the impact of melting temperature of these glasses on their luminescence properties was studied in detail. The reported observations allow the conclusion that Bi atoms (rather than clusters) are responsible for photoluminescence in the NIR spectral range.

2. Experimental details

Glass samples were synthesized by conventional melting and quenching of mixtures of analytical reagents H_3BO_3, SiO_2, Sb_2O_3, PbO and Bi_2O_3. Selected glass compositions (in wt%) were $54Bi_2O_3{\cdot}24B_2O_3{\cdot}5SiO_2{\cdot}17PbO$ (BG1) and $52Bi_2O_3{\cdot}23B_2O_3{\cdot}4SiO_2{\cdot}17PbO{\cdot}4Sb_2O_3$ (BG2). Individual batches of 60 g BG1 were melted at 1000–1300 °C (in steps of 100 K) for 30 min in corundum crucibles before being cast onto a stainless steel plate. Subsequently, the glass was annealed at 300 °C for 1 h. Similarly, 60 g of batch BG2 were produced after melting at 1100 °C for 30 min. Sample nomenclature is BG1@1000, BG1@1100, BG1@1200 and BG1@1300 for glasses of composition BG1 melted at 1000 °C, 1100 °C, 1200 °C and 1300 °C, respectively, and BG2@1100 for glass BG2. All samples were cut and mechanically polished into suitable shapes for optical analyses and further characterization.

In a first step, x-ray diffraction patterns of the glass samples were recorded using a Siemens Kristalloflex D500 x-ray diffractometer at 30 kV/30 mA, Cu Kα(λ = 1.5405 Å) at a scan rate of 1° min^{-1} over a 2Θ range of 5°–70°. For measuring optical absorption spectra, a JASCO V-570 spectrophotometer was employed. In order to study the NIR emission mechanism of Bi-doped glasses, diffuse reflection spectra of $NaBiO_3$ and Bi_2O_3 were measured with a Hitachi U-4100 spectrophotometer. NIR photoluminescence spectra and fluorescence decay curves were obtained using the set-ups described in [27, 28]. Microstructural characterization was performed by scanning electron microscopy (SEM, Quanta 200, FEI, Prag, Czech Republic, operated at 20 kV) in backscattering electron (BSE) mode and transmission electron microscopy (TEM, CM30, Philips, The Netherlands, operated at 300 kV). The elemental composition was determined by energy dispersive x-ray spectrometry (TEM–EDS) in the TEM equipped with an SiLi detector (7370 ISIS 30, Link, UK). Individual Bi nanoparticles were selected in the scanning transmission electron microscopy (STEM) mode for EDS point analysis. All measurements were taken at room temperature. Due to the low melting point of Bi (271.5 °C), selected-area electron diffraction (SAED) did not produce useful data.

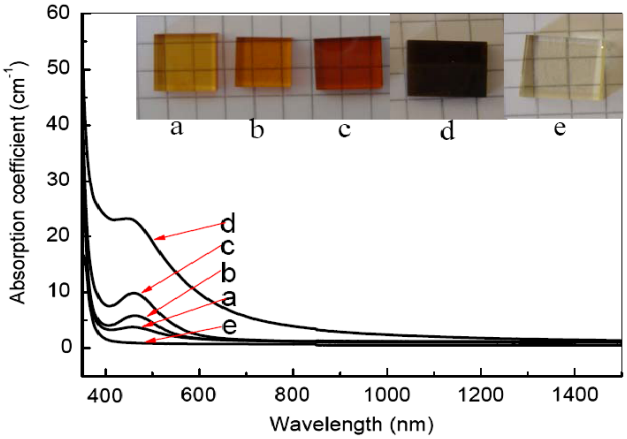

Figure 1. Absorption spectra of BG1 glasses melted at different temperatures: (a) 1000 °C, (b) 1100 °C, (c) 1200 °C and (d) 1300 °C. Curve (e) is the absorption spectrum of BG2 glass melted at 1100 °C. The inset is the photography of glasses (a)–(e).

3. Results and discussion

Figures 1(a)–(d) show absorption spectra of BG1 glasses prepared at different temperatures. As shown in figure 1(a), there is a broad absorption peak at ∼465 nm in the spectrum of BG1@1000. As the melting temperature increases further, the position of this peak remains unchanged, but the absorption coefficient (peak area) gradually increases from 3.89 to 22.64 cm^{-1}, implying increasing concentration of the active center(s). Correspondingly, the color of the glass sample turns from light brown, to reddish brown and then to black, as shown in the inset of figure 1. Upon excitation of these samples with 785 nm laser radiation (∼100 mW), broad NIR emission with peak intensity at ∼1230 nm can be observed from all samples (figure 2). Here, too, the position of the peak remains unchanged with changing melting temperature, but intensity shows a strong dependence. As melting temperature

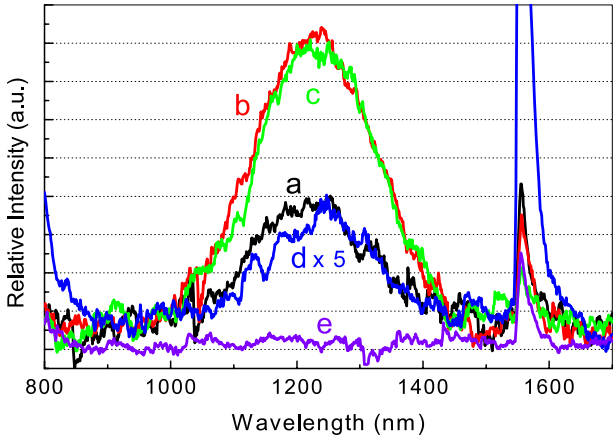

Figure 2. NIR emission spectra of BG1 glasses melted at different temperatures when pumped by 100 mW 785 nm laser diode: (a) 1000 °C, (b) 1100 °C, (c) 1200 °C, (d) 1300 °C and (e) BG2@1100. The spectrum (d) of BG1 is magnified by five times.

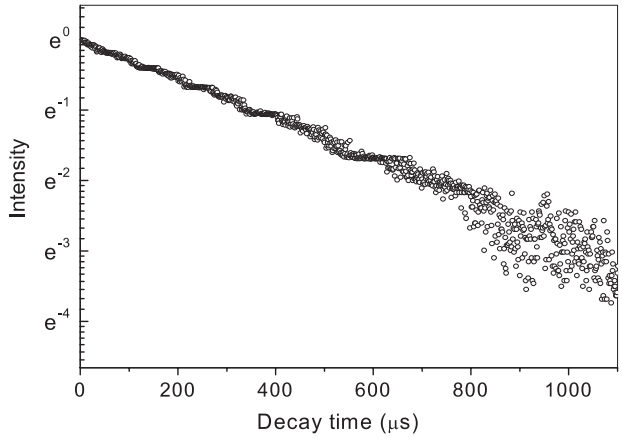

Figure 3. Fluorescent decay curve of BG1@1200 when pumped by 785 nm laser diode. The monitoring emission wavelength is 1230 nm.

is increased, NIR emission of the glasses first intensifies and attains a maximum between 1100 and 1200 °C. Melting above 1200 °C, however, results in significantly weakened NIR emission.

Fluorescence decay curves (lifetime) were measured for BG1@1100 and BG1@1200 (dynamic measurements on BG1@1000 and BG1@1300 were unsuccessful due to insufficient emission intensity). Figure 3 presents the decay curve of BG1@1200. Fitting decay curves to a first-order exponential decay equation results in lifetimes of 391 μs and 358 μs for BG1@1100 and BG1@1200, respectively. The decrease in lifetime from BG1@1100 to BG1@1200 is attributed to concentration quenching arising from increased concentration of emission centers as shown in figure 1 (curves (b) and (c)).

Comparing absorption, emission and fluorescence lifetimes of BG1 glasses with Bi-doped glasses that show broad NIR emission it can be concluded that the responsible emission centers are equivalent [8–19, 23–28].

XRD patterns are similar for all five glasses. All patterns show the characteristic glass hump, but no sharp diffraction peak that would indicate the presence of crystalline phases of significant volume fraction and size. On a first view SEM analyses (figure 4) reveal the same picture except for BG1@1300. In this sample, the presence of nanoscopic heterogeneities is clearly visible (bright spots in figure 4(b)). The diameter of these heterogeneities varies in the range of 100–150 nm. After scanning four different areas on the surface of BG1@1300, a distribution density of 5–7 particles/100 μm^2 was estimated. Considering the particle size, this is outside the detection limit of the employed XRD equipment. For this reason, TEM was used to further characterize the sample BG1@1300. STEM imaging (figure 5) shows a nanoheterogeneity with a diameter of ∼120 nm in BG1@1300. EDS oxygen mapping reveals an oxygen-(O) deficient valley in the center of figure 5(b) while, in the same area, the EDS map exhibits abundant protrusion of Bi (figure 5(c)). To more clearly characterize this observation, a TEM–EDS line scan

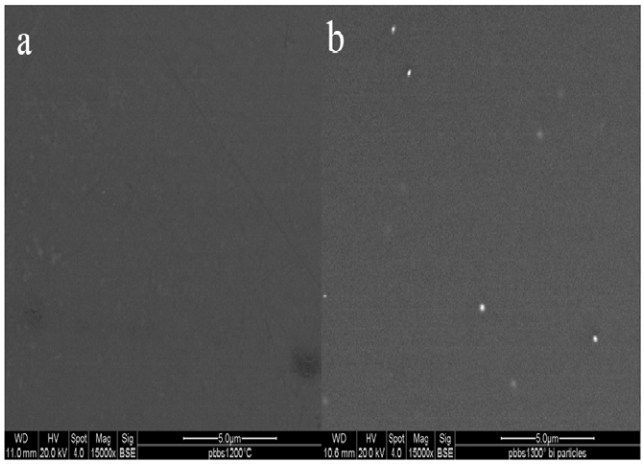

Figure 4. SEM images of BG1 glasses melted at (a) 1200 °C and (b) 1300 °C, respectively.

was performed (figure 6). The scan was started at position S and stopped at position E (figure 6), crossing the diameter of the heterogeneity. Micro-EDS spectra (figures 5(d) and (e), measurement positions indicated in figure 5(a), spot diameter ∼8 nm) reveal the presence of Pb, Bi and O elements in position 1 outside the heterogeneity and only Bi in position 2 inside the heterogeneity. The measurement at position 1 is consistent with the composition of BG1 (note that the Al peak is an artifact, originating from contamination by the corundum crucible, and Mo originates from the sample holder). From these observations, it can be concluded that the heterogeneities are colloids of Bi. The presence of these colloids is the reason for the dark color of BG1@1300 (the inset of figure 1).

Formation of the observed particles occurs according to the following reactions:

$$Bi_2O_3 \xrightarrow{1000-1300\,^\circ C} 2Bi + \tfrac{3}{2}O_2\uparrow \quad (1)$$

$$n\mathrm{Bi} \xrightarrow{1300\,^\circ C} \mathrm{Bi}_n(\text{nanoparticles}). \quad (2)$$

With increasing melting temperature, the concentration of the thermal dissociation product (Bi atoms) increases. The

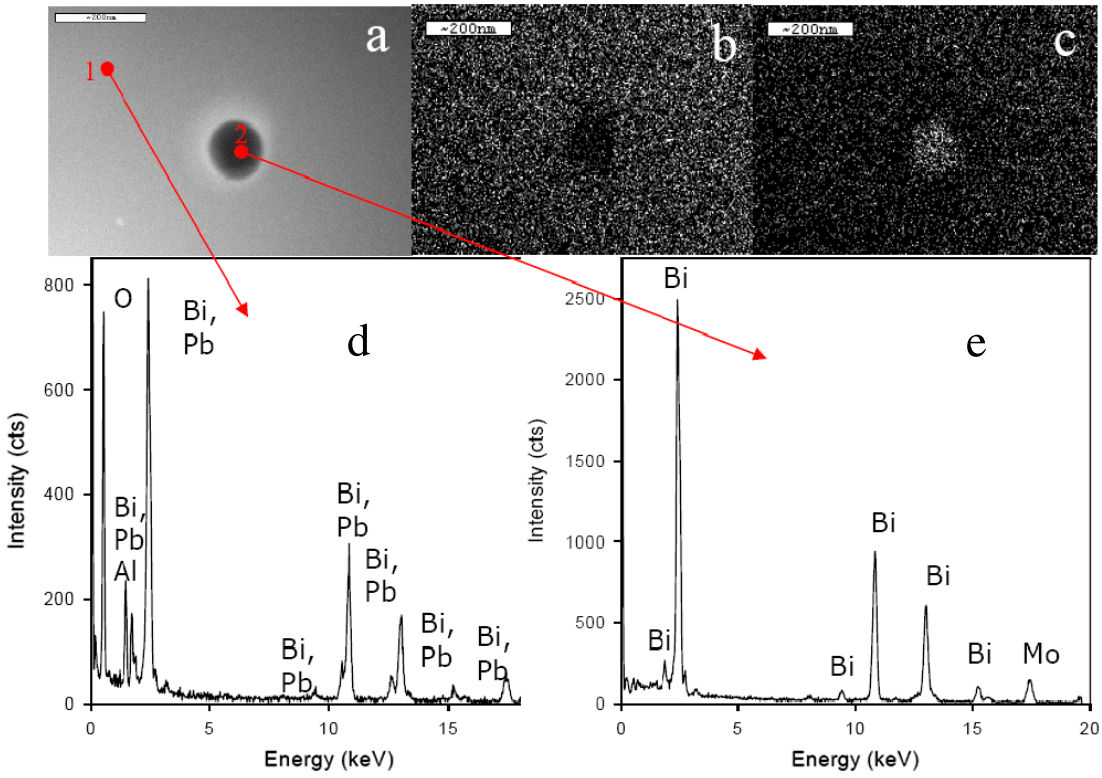

Figure 5. (a) TEM image, (b) EDS O map, (c) EDS Bi map, (d) EDS spectrum of spot 1 in image (a) and (e) EDS spectrum of spot 2 in image (a) of BG1 glass melted at 1300 °C. Spots 1 and 2 are ∼8 nm in diameter. The scale bars on images (a)–(c) are ∼200 nm.

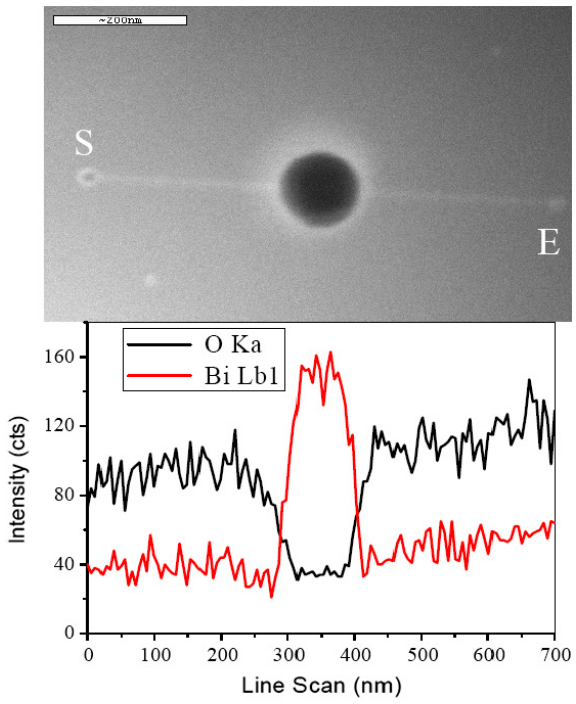

Figure 6. Bi (red line) and oxygen O (black line) concentration distribution along the line starting at spot S and ending at spot E as shown in the TEM image (top).

formation of nanoparticles (agglomeration) becomes more probable when the solubility limit of the melt is exceeded. No nanoparticles but strong NIR emission (figure 2) could be observed in samples BG1@1000–1200 (note that the absence of nanoparticles is also indicated by figure 1 due to the virtual absence of Mie scattering in the absorption curves of the first three samples as compared to BG1@1300). Thus, Bi nanoparticles are not the origin of NIR emission. Instead, as will be discussed in the following sections, results hint at elementary Bi dissolved in the glass matrix.

Atomic spectral data reveal [29] that the lowest excited electronic states of Bi^{5+} and Bi^{3+} (in the gas phase) are placed at 149 495 cm^{-1} and 70 963 cm^{-1}, respectively. That is why in the vis–NIR no absorption occurs in $NaBiO_3$ and Bi_2O_3, as shown in figure 7. If the Bi^{5+} ion was the NIR emission center in BG1@1300, it would not coexist with Bi atoms or nanoparticles since the Bi^{5+} ion has a strong oxidation capacity and would oxidize these species to higher valence states, e.g. Bi^{3+}. In the present case, Bi^{5+} ions can therefore not be the NIR emission centers, which is consistent with literature data on other Bi-doped glasses [9, 11–20, 23–27].

After exclusion of Bi^{3+} and Bi^{2+}, Meng *et al* [17, 18] proposed Bi^{+} as the species of interest. They assigned the absorption bands at ∼500 nm (20 000 cm^{-1}), 700 nm (14 286 cm^{-1}), 800 nm (12 500 cm^{-1}) and 1000 nm (10 000 cm^{-1}) to $^3P_0 \rightarrow {}^1S_0$, $^3P_0 \rightarrow {}^1D_2$, $^3P_0 \rightarrow {}^3P_2$ and $^3P_0 \rightarrow {}^3P_1$, and the emission in the 1.0–1.6 μm range to $^3P_1 \rightarrow {}^3P_0$. They did not assign the absorption band at ∼320 nm (figure 7(c)). Comparing this previous assignment to atomic spectral data of Bi^{+} (gas phase) reveals that it should be reconsidered. The energy states of $^1S_0$, $^1D_2$, $^3P_2$ and $^3P_1$ are located at 44 173 cm^{-1} (226 nm), 33 936 cm^{-1} (295 nm), 17 030 cm^{-1} (587 nm) and 13 324 cm^{-1} (751 nm)

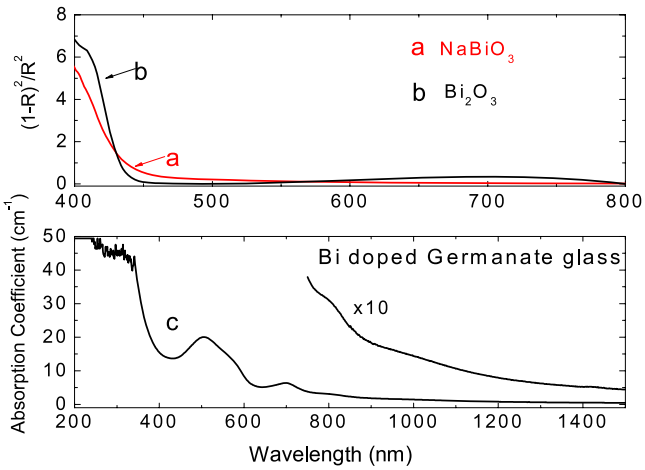

Figure 7. Diffuse reflection spectra of $NaBiO_3$ (Bi^{5+}) and Bi_2O_3 (Bi^{3+}) and absorption spectrum of $96.5GeO_2{\cdot}3Al_2O_3{\cdot}0.5Bi_2O_3$ glass where the spectral region of 750–1500 nm is magnified 10 times for clarity.

Table 1. Configuration, designations and energy levels of Bi^+ (electronic configuration: $1s^22s^22p^63s^23p^63d^{10}4s^24p^64d^{10}4f^{14}5s^25p^65d^{10}6s^26p^2$) (taken from [29]).

Configuration	Designation	Level (cm^{-1})
$6p^2$	$6p^2\ {}^3P_0$	0.00
$6p^2$	$6p^2\ {}^3P_1$	13 324
$6p^2$	$6p^2\ {}^3P_2$	17 030
$6p^2$	$6p^2\ {}^1D_2$	33 936
$6p^2$	$6p^2\ {}^1S_0$	44 173
$6p^17s^1$	$6p^2\ {}^3P_0$	69 133
$6p^17s^1$	$6p^2\ {}^3P_1$	76 147

(see table 1) [29]. If Bi^+ is introduced into solid materials, the excited energy levels may be lowered due to the enhanced interaction between activator and host (compared to the gas phase). However, the observed decrease should not be this large.

When comparing the atomic spectral data of Bi^0 with the observed absorption spectra of Bi-doped glasses, it is found that these match very well. As shown in table 2 [29], the ground state is $^4S_{3/2}$ and the energy levels of excited $^2P_{3/2}$, $^2P_{1/2}$, $^2D_{5/2}$ and $^2D_{3/2}$ are 33 164.84 cm^{-1} (302 nm), 21 661.0 cm^{-1} (462 nm), 15 437.66 cm^{-1} (648 nm) and 11 419.03 cm^{-1} (875 nm). As shown in figure 7(c), the absorption spectrum of Bi-doped germanate glass consists of five absorption bands (∼320 nm (31 250 cm^{-1}), ∼500 nm (20 000 cm^{-1}), 700 nm (14 286 cm^{-1}), 800 nm (12 500 cm^{-1}) and 1000 nm (10 000 cm^{-1})). When Bi^0 is introduced into solid oxide glasses, the excited levels will be relatively lowered and the first excited state of $^2D_{3/2}$ will be split into two sublevels $^2D_{3/2}(1)$ and $^2D_{3/2}(2)$ (crystal field splitting [30, 31]) as Bi^{2+} does in SrB_4O_7 [6] where the first excited state of $^2P_{3/2}$ is divided into the two sublevels $^2P_{3/2}(1)$ and $^2P_{3/2}(1)$. Therefore, the five observed absorption bands in Bi-doped glasses (see above) should be assigned to transitions from $^4S_{3/2}$ to $^2P_{3/2}$, $^2P_{1/2}$, $^2D_{5/2}$, $^2D_{3/2}(2)$ and $^2D_{3/2}(1)$, respectively.

Table 2. Configuration, designations and energy levels of atomic Bi (electronic configuration: $1s^22s^22p^63s^23p^63d^{10}4s^24p^64d^{10}4f^{14}5s^25p^65d^{10}6s^26p^3$) (taken from [29]).

Configuration	Designation	Level (cm^{-1})
$6p^3$	$6p^3\ {}^4S_{3/2}$	0.00
$6p^3$	$6p^3\ {}^2D_{3/2}$	11 419.03
$6p^3$	$6p^3\ {}^2D_{5/2}$	15 437.66
$6p^3$	$6p^3\ {}^2P_{1/2}$	21 661.0
$6p^3$	$6p^3\ {}^2P_{3/2}$	33 164.84

Correspondingly, the NIR emission can be attributed to $^2D_{3/2}(1) \rightarrow {}^4S_{3/2}$.

Bi colloids exhibit surface plasmon resonance absorption at 250–350 nm, depending on particle size [32–34]. The absorption and emission bands (BG1) at 465 nm and 1230 nm, respectively, can therefore be assigned to the transitions $^4S_{3/2} \rightarrow {}^2P_{1/2}$ and $^2D_{3/2}(1) \rightarrow {}^4S_{3/2}$ in elemental Bi. It is noteworthy that Bishay observed similar broad absorption at 515 nm due to elementary Bi in bismuth borate glass after γ-irradiation [35]. As shown by Peng *et al*, γ-irradiated bismuth borate glass indeed exhibits NIR emission at ∼1300 nm with FWHM = 236 nm [14].

Even though transitions such as $^4S_{3/2} \rightarrow {}^2D_{3/2}$ or $^2D_{5/2}$ are in principle parity- and spin-forbidden, the odd crystal field terms lead to an orbital admixture of higher energy states like ^2P and ^2D into the $^4S_{3/2}$ state [30]. That is why Bi^0 absorption at 870 nm (11 500cm^{-1}), 644 nm (15 527 cm^{-1}) and 458 nm (21 825 cm^{-1}) could be observed in a solid Ne matrix [31, 36]. The reported lifetime of the first excited state $^2D_{3/2}$ was reported to be 690 μs [30], which is of the same magnitude as the lifetime of NIR emission observed in Bi-doped glasses (e.g. 630 μs in Bi-doped aluminosilicate glass [8, 10] and 254 μs in Bi-doped germanate glasses [12]) as well as the bismuthate glasses of the present study. It was also reported that excitation of higher lying levels of Bi atoms always results in a fast nonradiative relaxation into the lowest excited $^2D_{3/2}$ electronic state [31]. That exactly agrees with results that have been reported for other Bi-doped glasses. For instance, NIR emission is commonly observed in the spectral range of 1.0–1.6 μm while continuously changing excitation light from 200 to 800 nm [28].

Ren *et al* [37] proposed BiO molecules dispersed in silicate glass as NIR emission centers, but successive work on Bi-doped chalcogenide glass rejected [19] this possibility because of the absence of oxygen in these glasses. More recently, it was demonstrated by the authors that in similar glasses NIR emission centers can be formed by femtosecond laser irradiation without additional thermal treatment [27]. Considering the short interaction time (∼330 fs) between the femtosecond laser and glass, it was concluded that diffusion-driven formation of Bi-containing clusters cannot occur in this case and that Bi-clusters are not a necessity for NIR emission.

Taking into account all the above arguments, it is now concluded that elementary bismuth, Bi^0, is the most probable NIR emission center in Bi-containing glasses.

By introducing oxidizing agents such as antimony oxide (Sb_2O_5) into the glass [38], Bi^0 can be oxidized to higher

valence states. Then, NIR emission will be eliminated as follows:

$$Sb_2O_3 + O_2(\text{dissolved}) \xrightarrow{1100\,^\circ C} Sb_2O_5 \quad (3)$$

$$3Sb_2O_5 + 4Bi^0 \xrightarrow{1100\,^\circ C} 3Sb_2O_3 + 2Bi_2O_3. \quad (4)$$

It is known [39] that the 5+ state of antimony is preferred below 1200 °C while the 3+ state is more stable at higher temperatures. Therefore, Sb_2O_3 was used as the antimony source in sample BG2@1100. Upon melting, antimony is further oxidized to Sb^{5+} at ∼1100 °C (equation (3)). Sb^{5+} subsequently acts as a redox partner for Bi^0, oxidizing it to Bi^{3+} (equation (4)). This leads to the light yellow color of sample BG2@1100 and, as expected, the absence of any NIR emission from this glass (figure 2(e)).

4. Conclusions

We reported on the NIR absorption and emission properties of bismuthate glass and their dependence on melting temperature. Results clarify that NIR emission occurs from the same centers as it does in Bi-doped glasses, and that these centers are Bi^0 species. By comparing with atomic spectral data, absorption bands at ∼320, ∼500, 700, 800 and 1000 nm are assigned to Bi^0 transitions $^4S_{3/2} \rightarrow {}^2P_{3/2}$, $^4S_{3/2} \rightarrow {}^2P_{1/2}$, $^4S_{3/2} \rightarrow {}^2D_{5/2}$, $^4S_{3/2} \rightarrow {}^2D_{3/2}(2)$ and $^4S_{3/2} \rightarrow {}^2D_{3/2}(1)$, respectively, and broadband NIR emission is due to the transition $^2D_{3/2}(1) \rightarrow {}^4S_{3/2}$.

The dependence of absorption and NIR emission of bismuthate glasses on melting temperature is interpreted as thermal dissociation of Bi_2O_3 into elementary Bi. Darkening of bismuthate glass melted at 1300 °C is due to Bi atom coagulation into spherical nanoparticles at 1300 °C. The presence of Bi nanoparticles is confirmed by SEM, TEM, STEM, high-resolution EDS and element distribution mapping. By adding antimony oxide as an oxidation agent to the glass, NIR emission centers can be eliminated and Bi^{3+} is formed.

Acknowledgments

Financial support by the Deutsche Forschungsgemeinschaft (DFG) under grant no. WO 1220/2-1 is gratefully acknowledged. The authors would like to thank Mrs Eva Springer and Mrs Hana Strelec for their assistance with SEM and XRD measurements, respectively.

References

[1] Blasse G 1988 *Prog. Solid State Chem.* **18** 79–171
[2] Blasse G and Brill A 1967 *J. Chem. Phys.* **47** 1920–6
[3] Blasse G and Brill A 1968 *J. Chem. Phys.* **48** 217–22
[4] Reisfeld R and Kalisky Y 1977 *Chem. Phys. Lett.* **50** 199–201
[5] Parke S and Webb R 1973 *J. Phys. Chem. Solids* **34** 85–95
[6] Blasse G, Meijerink A, Nomes M and Zuidema J 1994 *J. Phys. Chem. Solids* **55** 171–4
[7] Srivastava A 1998 *J. Lumin.* **78** 239–43
[8] Murata K, Fujimoto Y, Kanabe T, Fujita H and Nakatsuka M 1999 *Fusion Eng. Des.* **44** 437–9
[9] Peng M, Qiu J, Chen D, Meng X and Zhu C 2005 *Opt. Express* **13** 6892–8
[10] Fujimoto Y and Nakatsuka M 2001 *Japan. J. Appl. Phys.* **40** L279–81
[11] Suzuki T and Ohishi Y 2006 *Appl. Phys. Lett.* **88** 191912
[12] Peng M, Qiu J, Chen D, Meng X, Yang L, Jiang X and Zhu C 2004 *Opt. Lett.* **29** 1998–2000
[13] Peng M, Meng X, Qiu J and Zhao Q 2005 *Chem. Phys. Lett.* **403** 410–4
[14] Peng M, Qiu J, Chen D, Meng X and Zhu C 2005 *Opt. Lett.* **30** 2433–5
[15] Peng M, Wang C, Chen D, Qiu J, Jiang X and Zhu C 2005 *J. Non-Cryst. Solids* **351** 2388–93
[16] Peng M, Wu B, Da N, Wang C, Chen D, Zhu C and Qiu J 2008 *J. Non-Cryst. Solids* **354** 1221–5
[17] Meng X, Qiu J, Peng M, Chen D, Zhao Q, Jiang X and Zhu C 2005 *Opt. Express* **13** 1635–42
[18] Meng X, Qiu J, Peng M, Chen D, Zhao Q, Jiang X and Zhu C 2005 *Opt. Express* **13** 1628–34
[19] Ren J, Chen D, Yang G, Xu Y, Zeng H and Chen G 2007 *Chin. Phys. Lett.* **24** 1958–60
[20] Dianov E, Dvoyrin V, Mashinsky V, Umnikov A, Yashkov M and Gur'yanov A 2005 *Quantum Electron.* **35** 1083–4
[21] Ohkura T, Fujimoto Y, Nakatsuka M and Young-Seok S 2007 *J. Am. Ceram. Soc.* **90** 3596–600
[22] Duffy J 1993 *Geochim. Cosmochim. Acta* **57** 3961–70
[23] Peng M, Chen D, Qiu J, Jiang X and Zhu C 2007 *Opt. Mater.* **29** 556–61
[24] Arai Y, Suzuki T and Ohishi Y 2007 *Appl. Phys. Lett.* **90** 261110
[25] Truong V, Bigot L, Lerouge A, Douay M and Razdobreev I 2008 *Appl. Phys. Lett.* **92** 041908
[26] Khonthon S, Morimoto S, Arai Y and Ohishi Y 2007 *J. Ceram. Soc. Japan* **115** 259–63
[27] Peng M, Zhao Q, Qiu J and Wondraczek L 2009 *J. Am. Ceram. Soc.* **92** 542–4
[28] Peng M and Wondraczek L 2009 *J. Mater. Chem.* **19** 627–30
[29] Moore C 1971 *Atomic Energy Levels Nat. Bur. Stand. (US)* vol 35/V.III (Washington, DC: US Government Printing and Publishing Office) pp 219–26
[30] Goovaerts E, Nistor S and Schoemaker D 1990 *Phys. Rev.* B **42** 3810–7
[31] Bondybey V, Schwartz G, Griffiths J and English J 1980 *Chem. Phys. Lett.* **76** 3–4
[32] Radhakrishna S and Srinivasa R 1976 *Phys. Rev.* B **14** 969–76
[33] Fang J, Stokes K, Weimann J, Zhou W, Dai J, Chen F and O'Connor C 2001 *Mater. Sci. Eng.* B **83** 254–7
[34] Gutiérrez M and Henglein A 1996 *J. Phys. Chem.* **100** 7656–61
[35] Bishay A 1961 *Phys. Chem. Glasses* **2** 33–8
[36] Tel-Dan R, Bachar J and Rosenwaks S 1986 *Chem. Phys. Lett.* **126** 510–5
[37] Ren J, Yang L, Qiu J, Chen D, Jiang X and Zhu C 2006 *Solid State Commun.* **140** 38–41
[38] Day F Jr and Silverman A 1942 *J. Am. Ceram. Soc.* **25** 371–81
[39] Pye L, Stevens H and LaCourse W 1972 *Introduction to Glass Science* (New York: Plenum) p 291